

Phonon anomalies and range of superconducting energy gaps from infrared studies of $\text{YBa}_2\text{Cu}_3\text{O}_{7-\delta}$

L. Genzel, A. Wittlin,* M. Bauer, M. Cardona, E. Schönerr, and A. Simon

Max-Planck-Institut für Festkörperforschung, Heisenbergstrasse 1, D-7000 Stuttgart 80, Federal Republic of Germany

(Received 3 January 1989)

The infrared reflectivity of sintered $\text{YBa}_2\text{Cu}_3\text{O}_{7-\delta}$, prepared under carefully controlled oxidation conditions, has been measured between 20 and 10000 cm^{-1} at temperatures between 10 and 300 K. In this paper we analyze in detail the temperature- and frequency-dependent far-infrared part of the spectrum. A Kramers-Kronig analysis allows us to compare the phonon part of the spectra with lattice-dynamical calculations. There is fairly good agreement concerning the assigned eigenfrequencies. The oscillator strengths of the experimentally observed phonons, however, are all stronger than those from a lattice-dynamics model which assumes ionic charges close to the formal ones. This is especially so for the lowest phonon found at 155 cm^{-1} which shows a strength $S = 60 \pm 5$ being about 15 times higher than theoretically expected. A possible origin of this effect is discussed qualitatively in terms of a Cu(1)-O(IV) charge shift during the vibration induced by the polarization field. The electronic background of the spectra has been analyzed by a Mattis-Bardeen type of dielectric response below T_c . The best fit yielded, for low T , a gap distribution in the range from about 160 to 370 cm^{-1} , corresponding to $2\Delta(0)/k_B T_c$ values between 2.6 and 6.0.

I. INTRODUCTION

Experimental studies of the far-infrared (FIR) reflectance in the superconducting $\text{YBa}_2\text{Cu}_3\text{O}_{7-\delta}$ have produced numerous results.¹⁻⁸ Due to constant progress in the quality of the ceramic superconducting samples and their characterization, the FIR data obtained recently in various laboratories now agree quite well, but there still remain some uncertainties in their interpretation, especially concerning the position of the energy-gap region. Since the available single crystals of $\text{YBa}_2\text{Cu}_3\text{O}_{7-\delta}$ are still rather small for reliable FIR measurements, their studies were concentrated mainly on the middle and near infrared where, similar to the ceramic material, a broad and temperature-independent reflectance band around 3000 cm^{-1} is found which disappears in the nonmetallic $\text{YBa}_2\text{Cu}_3\text{O}_6$ phase. The FIR spectra of superconducting $\text{YBa}_2\text{Cu}_3\text{O}_{7-\delta}$ ceramics show a very pronounced phonon structure in contrast to films and single crystals of this material which have the c axis perpendicular to the reflecting surface. This may indicate that the phonons observed are only those with their eigenvector in the c direction, while a - b phonons do not show up due to the high electronic screening if the electric vector lies in the a - b plane.

The existence of lattice-dynamical calculations⁹ allowed us to assign most of the phonons observed in the FIR and by Raman scattering.¹⁰ This assignment could be supported by replacing the yttrium by most of the rare-earth metals^{11,12} and by the partial substitution¹³ of ^{16}O by ^{18}O .

In the present paper, we report measurement of the temperature and frequency dependence of the infrared reflectance of ceramic $\text{YBa}_2\text{Cu}_3\text{O}_{7-\delta}$ with emphasis on locating the energy-gap region and on the quantitative

analysis of the position and strengths of the phonons in comparison with lattice dynamics. The paper is organized as follows: In Sec. II we describe the sample preparation and characterization. The infrared spectra and their Kramers-Kronig (KK) analysis are presented in Sec. III. Section IV describes the detailed investigation of the phonon response, while Sec. V is devoted to the electronic behavior.

II. EXPERIMENTAL

High-purity (99.999%) powders (Alfa Products, Morton Thiokol Co. Inc., USA) of Y_2O_3 , BaCO_3 , and CuO were used as starting materials. Each compound was heated in air at 400°C for about 6 h to remove moisture

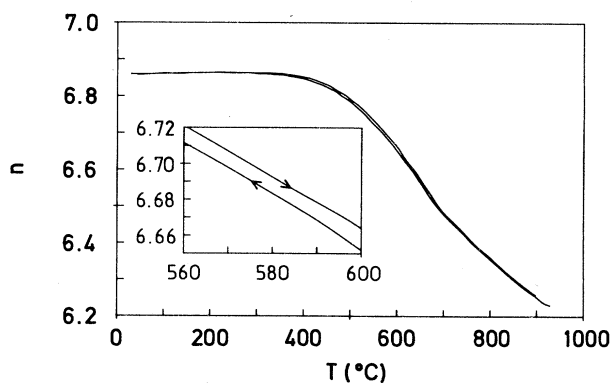


FIG. 1. Oxygen coefficient n of $\text{YBa}_2\text{Cu}_3\text{O}_n$ as a function of temperature for heating ($1.9^\circ\text{C}/\text{min}$) and cooling ($1.5^\circ\text{C}/\text{min}$); the inset shows a magnified representation of the very small hysteresis loop.

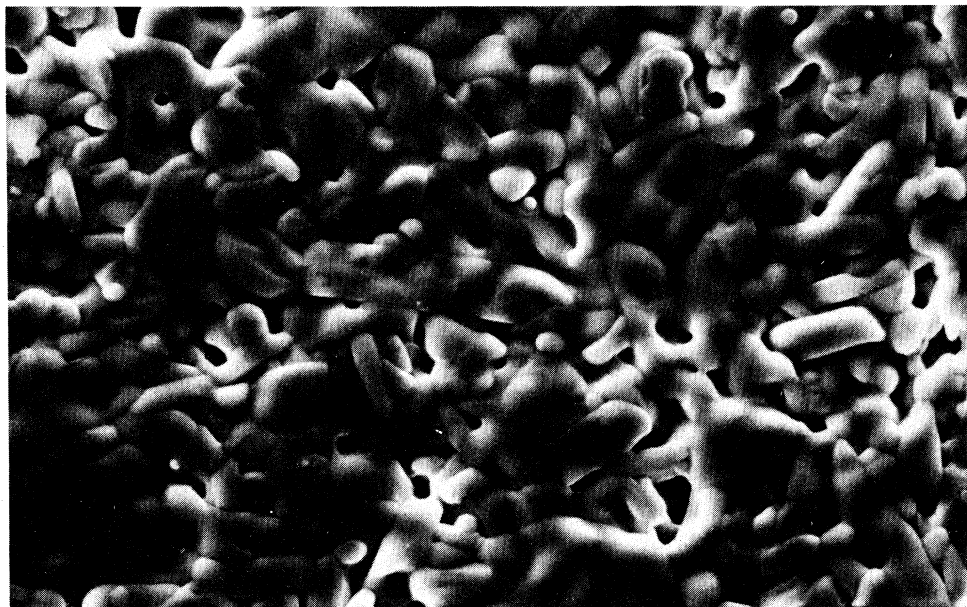


FIG. 2. Typical crystallite structure (6–20 μ size) at the sample surface; the horizontal width of the figure corresponds to 80 μ .

and to oxidize the CuO completely. A stoichiometric mixture of about 4 g was manually ground for at least half an hour with the help of a WC mortar and loaded afterwards onto a gold pan of a recording balance. The pan was hung in a vertical silica glass tube which was flooded with high-purity oxygen (99.999%) at a rate of 110 cm^3/min . For synthesis of the yttrium barium cuprate the material was heated to 928 $^\circ\text{C}$ at a rate of 2.2 $^\circ\text{C}/\text{min}$, fired at that temperature for 26 h and finally cooled to room temperature at a rate of 1.7 $^\circ\text{C}/\text{min}$. With the use of only 928 $^\circ\text{C}$, the formation of a liquid which might lead to undesired compounds was avoided. Under the assumption of complete CO_2 removal, the final weight indicated an oxygen deficiency of $\delta=0.60$ at the applied calcination temperature and $\delta=0.05$ at room temperature, respectively. When the reaction product was examined with an optical microscope it appeared uniformly black without any detectable green phase (Y_2BaCuO_5).

After extended manual grinding, the synthesized cuprate was pressed into pellets of 1 cm in diameter and thickness of 1–2 mm at a pressure of 8.8 kbar and heated at a rate of 1.9 $^\circ\text{C}/\text{min}$ to 937 $^\circ\text{C}$ under flowing 99.999% pure oxygen at a rate of 110 cm^3/min . After an annealing at that temperature for 48 h the sample was cooled to room temperature at a rate of 0.8 $^\circ\text{C}/\text{min}$. The oxygen deficiency changed during this procedure from $\delta=0.65$ at the beginning of firing to 0.76 at the end of firing and to 0.14 at room temperature. Again the values were calculated from the weight change under the assumption of completed CO_2 evolution. Thus the estimated high oxygen content of 6.95 for the synthesized cuprate powder is assumed to result from not completely evolved CO_2 . A second repeated heating cycle led to a nearly reversible oxygen exchange as shown in Fig. 1, where the

stoichiometry is drawn as a function of temperature for pure-oxygen environment at 1 atm. The values were obtained from weighing the sample whose initial oxygen coefficient had been estimated from the weight of the starting compounds. The derivative of the temperature-weight curve revealed a maximum rate of weight change at 655 $^\circ\text{C}$ and at $\delta=0.42$. Superconducting samples have been characterized by x-ray measurements, dc conductivity, and temperature dependence of magnetization measurements. All samples were orthorhombic with lattice constants $a=3.8195\pm 0.0008$, $b=3.8886\pm 0.0008$, and $c=11.6759\pm 0.0025$ \AA . They show superconducting

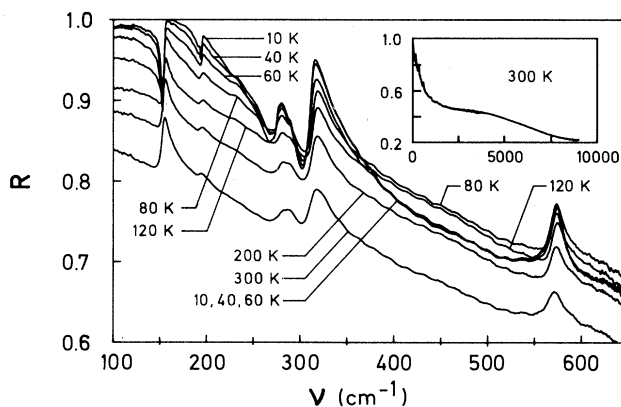


FIG. 3. FIR reflectivity at various temperatures between room temperature and 10 K; the inset shows the MIR and NIR range at 300 K. The data are normalized with respect to the reflectivity of the same sample after evaporation of a 5000- \AA gold layer.

transition at 89 K (zero resistance) and approximately 90% diamagnetic shielding at 10 K. The sample surface has been studied by electron scanning microscopy. A typical picture, shown in Fig. 2, reveals that the sample surface contains a large portion of small (6–20 μm) crystallites. Their orientation appears to be random. Therefore, we assume that the crystallites at the surface of our samples are not oriented.

III. RESULTS

The reflectance measurements were made at temperatures between 10 and 300 K over the range from 100 to 10 000 cm^{-1} with a Bruker IFS 113v interferometer. The reflectance measurements were performed with an aluminum mirror as well as with the gold-coated sample as a reference. In the 20–650 cm^{-1} region a medium-pressure Hg arc as source and a He-cooled silicon bolometer as a detector were used. They were replaced in the 400–5000 cm^{-1} region by a global source and a deuterated triglycine sulfate detector and above this region by a tungsten lamp and an InSb photodetector. The data from different source-detector setups showed a mismatch of about 5%. Since the FIR spectra are most important for the KK analysis, we slightly scaled the high-frequency reflectance data to produce a smooth spectrum. More serious are errors in the absolute reflectance R in the low-frequency range below 100 cm^{-1} which occur even if the gold-coated sample was used as a reference. It is difficult to reduce the error of different measurements of R to less than $\pm 2\%$. The KK analysis reacts to this with rather serious artifacts below 100 cm^{-1} (see also Ref. 8). We should mention that an extensive study of $\text{YBa}_2\text{Cu}_3\text{O}_{7-\delta}$, which we performed in the mm-wave spectral range, yielded even at He temperatures an absorption $A = 1 - R$ of the order of 1%; similar results have been reported by other groups also.¹⁴ We will publish these results elsewhere since they seem not to interfere too much with the results of this paper, although they may be of vital importance for applications of the superconductors.

We, therefore, extrapolated the reflection data below 100 cm^{-1} with a Mattis-Bardeen fit (see Sec. V). A typical result of a reflectance measurement in the range from 100 to 650 cm^{-1} and at several temperatures between 10 and 300 K is shown in Fig. 3. The inset gives the 300-K reflectance spectrum up to about 10 000 cm^{-1} . Except for smaller differences of the absolute R values and details of the phonon features, our data are similar to those published by other groups.^{3,8}

In order to extract the physical information from the reflectance data, two methods can be used: a KK analysis,¹⁵ and a fit with the help of a model dielectric function. We used the first method to extract the phonon information and then the second for the interpretation of the electronic part of the KK analysis. Figure 4 shows the frequency dependence of the real part σ_1 of the conductivity between 100 and 650 cm^{-1} and for 10 and 120 K, according to the KK analysis of the data of Fig. 3.

In Fig. 5 we present the KK data of σ_1 for 10 K with

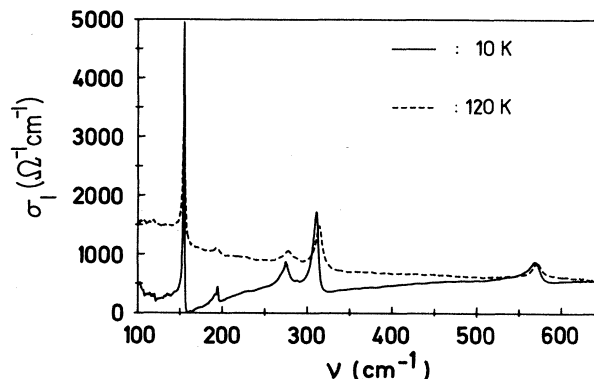


FIG. 4. σ_1 obtained by KK analysis of the data presented in Fig. 3 above (120 K) and below (10 K) T_c .

extended frequency scales around the phonon structures. It is apparent that all phonon modes show some asymmetry which is probably caused by the Fano effect.¹⁶ In the case of the 155- cm^{-1} mode, however, we find also an influence on the asymmetry of the aforementioned reflectance uncertainty at low wave numbers.

IV. PHONONS

The assignment of the TO-phonon modes of $\text{YBa}_2\text{Cu}_3\text{O}_{7-\delta}$ has been discussed by several authors.¹⁰

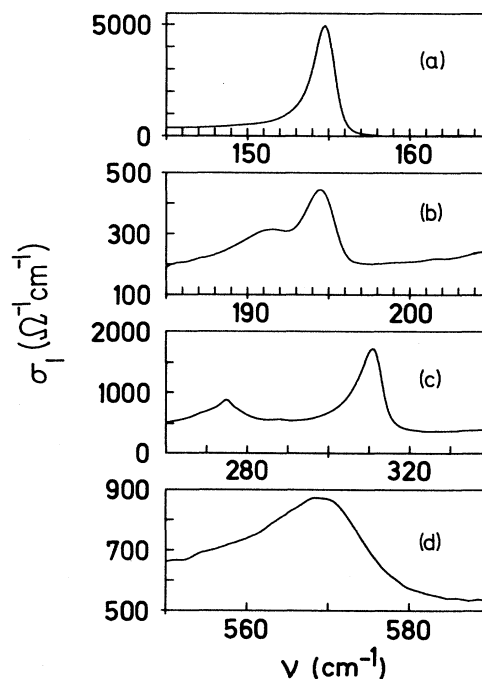


FIG. 5. Magnified representation of σ_1 at 10 K for the strongest phonon modes (KK analysis).

TABLE I. Experimental values of the phonon eigenfrequencies, half-widths, and oscillator strengths of $\text{YBa}_2\text{Cu}_3\text{O}_7$ for 10 K obtained by a Kramers-Kronig analysis.

ν_j (cm^{-1})	154.8	191.5	194.5	275	288	311	569
Γ (cm^{-1})	1.6–1.8	~ 2	~ 1.3	9		8	12–15
\bar{S}_j^a	19–22	~ 0.3	0.6–0.7	2.6–2.8	> 0.1	6.9–7.1	0.8–0.9

^aThe actual oscillator strengths are three times larger since the measurements were made on a nonoriented ceramic material.

In the present work we shall follow the assignment given in Ref. 17 and we will compare the measured eigenfrequencies and oscillator strengths with the lattice-dynamical calculation.⁹ Table I shows our observed phonon frequencies ν_j , half-widths Γ_j , and oscillator strengths \bar{S}_j at 10 K and Table II represents the same information, given in Ref. 8 at 2 K. It should be noted that our measurements were made on almost unoriented ceramic material with the consequence that \bar{S}_j in Table I is a spatial average of the actual oscillator strength S_j , thus yielding $S_j \approx 3\bar{S}_j$.

The result of the lattice-dynamical calculation concerning eigenfrequencies and relative displacements for four slightly different charge distributions $A-D$ (see Table III) is presented in Table IV together with calculated oscillator strengths. Our definition of the oscillator strength S_j of mode j is based on the contribution of that mode to the complex dielectric function

$$\Delta\hat{\epsilon}_j = \frac{S_j \nu_j^2}{\nu_j^2 - \nu^2 - i\nu\Gamma_j} \quad (1)$$

Due to the orthorhombic D_{2h} point-group symmetry of $\text{YBa}_2\text{Cu}_3\text{O}_{7-\delta}$ one finds from lattice dynamics that the eigenvectors of the various modes in X , Y , and Z directions are decoupled. Thus the oscillator strengths in Eq. (1) can be written as¹⁸

$$S_j = \frac{4\pi}{V_c} \frac{\left[\sum_k e_k \xi_{kj} \right]^2}{\sum_k m_k \xi_{kj}^2 \omega_j^2}, \quad (2)$$

where V_c is the volume of the unit cell, e_k and m_k are the charge and mass of the ion k , respectively, and ξ_{kj} represents the displacement of particle k in mode j . Equation (2) for S_j has been used for the calculated strengths of Table IV containing the important modes.

To compare this with experiment one first has to specify the assignment. Starting from the high-frequency end we attribute the observed mode at 569 cm^{-1} to the mode

labeled 12 in Table IV and the observed mode at 311 cm^{-1} to the mode labeled 11. In spite of the strength of the observed 275-cm^{-1} mode we assign it tentatively to the mode labeled 7, although the agreement between experimental and theoretical values is not particularly good. The observed phonon at 194.5 cm^{-1} is clearly identified as the “yttrium” mode, labeled 6, since it shifts drastically down by replacing the yttrium with the heavier rare-earth ions.¹¹ A weak phonon found at 191.3 cm^{-1} is not found as Z mode. The very strong and sharp phonon found at 154.8 cm^{-1} should best be assigned to the “barium” mode labeled 3, although some other assignment has been given in the literature.¹² The rather strong mode 1 of the calculation are not observed by us, probably because the reflectance is already so high that the phonon structures are suppressed.

A comparison of the observed and calculated strength S_j shows a remarkable discrepancy: All observed S_j are larger than the calculated ones and this is especially so for the “barium” mode at 154.8 cm^{-1} which appears to be 15 times stronger than calculated. This effect was pointed out before,⁸ as seen from Table II. There is no way of changing the formal charge distribution of $\text{YBa}_2\text{Cu}_3\text{O}_{7-\delta}$ in a reasonable way to get a strength of 60 for this mode. On the basis of local charges, one would have to assume a charge in excess of $24+$ for barium or $15-$ for the oxygen O(IV) to account for $S=60$ for the mode 3. Such values are chemically meaningless. An apparently similar problem was found for the ir spectra of the valence-fluctuating compound CePd_3 .^{19,20} An effective charge $10+$ for Pd was required to account for the experimentally observed oscillator strength of the stronger optical phonon in this compound. It seems more reasonable to associate the observed enhanced oscillator strength with dynamical changes of the electronic configurations of atoms, i.e., charge-transfer processes.

The Y and Ba atoms in the structure of $\text{YBa}_2\text{Cu}_3\text{O}_{7-\delta}$ behave rather like trivalent and divalent cations, as can be deduced from their temperature-dependent positional parameter shifts. In fact, one would expect that these electropositive elements in the highly oxidized system

TABLE II. Fit parameters of the phonon eigenfrequencies, half-widths, and oscillator strengths of $\text{YBa}_2\text{Cu}_3\text{O}_7$ for 2 K taken from Bonn *et al.* (Ref. 8).

ν_j (cm^{-1})	155	194	277	311	534	567
Γ (cm^{-1})	2.4	2.7	21	9	50	17
\bar{S}_j^a	31	2	10	12	3	2

^aWe assume that the oscillator strengths in this publication correspond to our definition of \bar{S}_j .

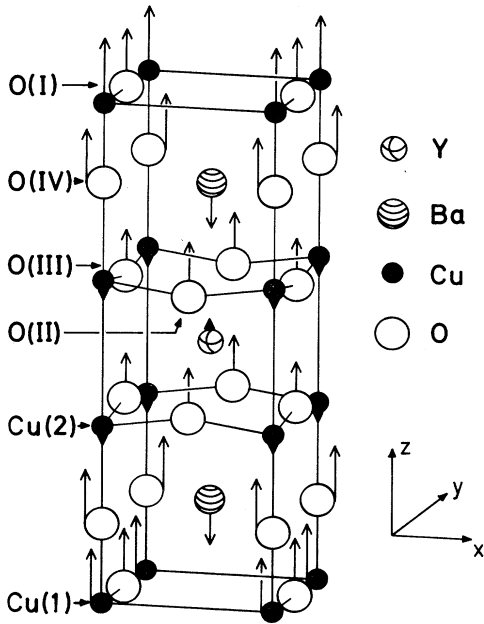


FIG. 6. Unit cell of $\text{YBa}_2\text{Cu}_3\text{O}_7$ with the relative atomic displacements of the "barium mode" at 154.8 cm^{-1} .

only act as valence-establishing spacers, which are electronically inert. Charge transfer should therefore occur only between the Cu and O atoms. The displacements of these atoms in the 154.8-cm^{-1} mode are such that the CuO_3 ribbon moves as a rigid unit (see Fig. 6). We assume that the charge distribution in the CuO_3 ribbon is

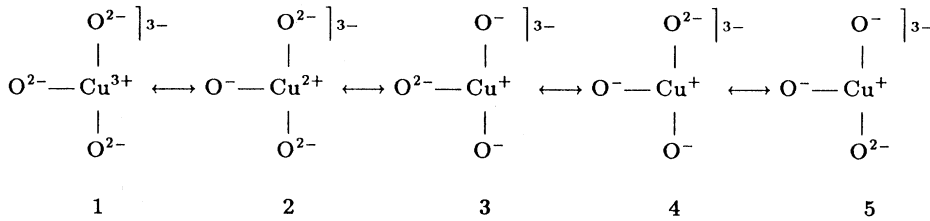


TABLE III. Formal local charge distributions of the ions in $\text{YBa}_2\text{Cu}_3\text{O}_7$ in units of the elementary charge.

	Cu(1)	Cu(2)	Ba	Y	O(I)	O(II)	O(III)	O(IV)
<i>A</i> ^a	2.0	2.0	1.9	2.85	-1.81	-1.81	-1.81	-1.81
<i>B</i>	2.25	2.0	2.0	3.0	-1.25	-2.0	-2.0	-2.0
<i>C</i>	2.50	2.0	2.0	3.0	-1.5	-2.0	-2.0	-2.0
<i>D</i>	2.75	2.0	2.0	3.0	-1.75	-2.0	-2.0	-2.0

^aThe set *A* of charges has been used in the lattice dynamical calculation.⁹ The variation of charges in *B*, *C*, *D* will have some minor influence on the eigenvectors given in Table IV.

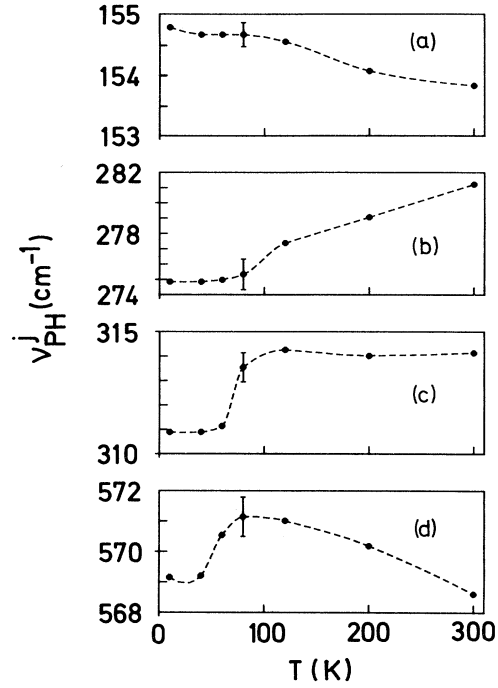


FIG. 7. Temperature dependence of the phonon frequencies ν_{PH}^j for the four strongest modes.

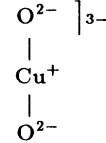
delicately influenced by the amount of displacement. The different configurations of the mesomeric system of the CuO_3 ribbon can be depicted for the unit of repetition, CuO_3^{3-} , in a formal ionic description, as seen below:

TABLE IV. Relative displacements and calculated oscillator strengths of $\text{YBa}_2\text{Cu}_3\text{O}_7$ according to the four different sets of charges given in Table III.

ν_j (cm^{-1})	Mode direction	Displacements ^a				S_j								
		Cu(1)	Cu(2)	Ba	Y	O(I)	O(II)	O(III)	O(IV)	A	B	C	D	
1	94.6	Z	2.1	-7.8	2.3	-0.7	4.0	3.0	2.5	2.0	9.4	9.3	9.4	9.6
2	120.3	X	4.5	2.4	-4.1	4.2	-12.3	2.5	3.0	-7.5	3.8	3.0	3.7	4.4
3	153.5	Z	6.6	-0.3	-3.8	1.3	5.0	4.0	3.5	6.5	4.0	4.2	4.1	4.1
4	169.9	X	-7.6	-0.3	0.9	2.3	16.5	-0.5	2.0	-5.5	0.5	0.2	0.3	0.6
5	197.7	X	-1.4	5.5	-0.6	-6.2	5.5	6.0	-5.0	-0.5	0.1	0.1	0.1	0.2
6	197.9	Z	5.2	1.4	1.2	-7.2	3.0	-6.0	-5.5	4.5	0.3	0.5	0.5	0.5
7	319.0	Z	1.2	-0.8	-0.2	2.3	-0.2	-18.6	15.6	0.0	0.02	0.07	0.07	0.08
8	349.9	Y	-1.4	-0.7	-0.9	-4.2	4.0	13.0	1.0	8.5	2.8	3.2	3.2	3.3
9	352.2	X	1.0	1.0	1.5	1.3	-8.5	0.5	-4.0	-14.5	2.1	2.2	2.3	2.4
10	356.3	X	0.3	0.0	0.3	-4.6	-2.5	1.0	15.5	-4.0	0.8	1.0	1.0	1.0
11	363.3	Z	-4.1	1.4	0.0	-6.2	3.5	7.0	10.5	1.0	1.9	2.2	2.2	2.3
12	509.0	Z	-6.9	-0.3	0.0	1.6	9.0	-3.0	-3.5	11.5	0.2	0.2	0.3	0.3
13	545.3	Y	0.3	-3.2	0.0	0.7	-1.0	-1.5	15.5	0.0	0.3	0.4	0.4	0.4
14	565.2	X	0.0	3.8	0.0	-0.3	0.0	-15.5	1.0	0.5	0.4	0.4	0.4	0.4

^aThe displacements are normalized according to $\sum_k m_k \xi_k^2 = 10^4$, $\xi = X, Y, Z$.

The configurations 1–3 contribute to the ground electronic state, while configurations 4 and 5 which actually involve the “peroxiton”^{21,22} may play an important role in the 154.8-cm^{-1} excited vibrational state. They exhibit a dipole in the c direction of the crystal and, if favored by a displacement of the CuO_3 ribbon in the c direction, could lead to the observed enhancement of strength for the 154.8-cm^{-1} mode. In $\text{YBa}_2\text{Cu}_3\text{O}_6$ the O(I) atoms between the Cu atoms are missing, thereby leaving the Cu atom with the d^{10} configuration of the Cu^+ ion:



Due to the closed-shell configuration of the Cu^+ ion the charge transfer between Cu and O is prohibited in agreement with the experimental finding that the strength of the corresponding mode (shifted to 168 cm^{-1}) (Ref. 23) is normal.

It has been pointed out earlier²⁴ that some phonons become soft below T_c and an attempt has been made to explain this effect within the framework of the strong-coupling theory.²⁵ We show in Fig. 7 our newest determination of the temperature dependence of the phonon positions. The softening is clearly apparent for the modes at 275 cm^{-1} , 311 cm^{-1} , and 569 cm^{-1} , while there is no clear effect seen for the 154.8-cm^{-1} mode. This may indicate, together with the very low half-width, that this phonon is at 10 K well below the essential gap region.

It is also remarkable that the S_j of all observed pho-

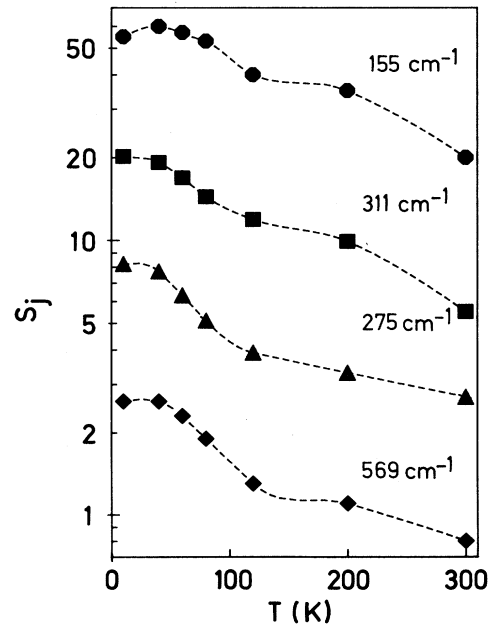


FIG. 8. Temperature dependence of the phonon oscillator strengths S_j for the modes shown in Fig. 7.

TABLE V. Fit parameters for the Mattis-Bardeen model dielectric function [Eq. (3)] used in Fig. 9. The parameters for the phonon Lorentzians are taken from the Kramers-Kronig analysis (Table I).

Critical temperature T_c	89 K
Nonsuperconducting part f_n of the sample at $T=0$	0.2
Superconducting energy gaps $\nu_{g1}(0)$ and $\nu_{g2}(0)$, each weighted with 50%	160 cm^{-1} 370 cm^{-1}
Plasma frequency ν_p	7400 cm^{-1}
Scattering frequency ν_r	750 cm^{-1}
Electronic oscillator:	
ν_e (cm^{-1})	3100
Γ_e (cm^{-1})	4000
S_e	50
ϵ_∞	4.7

nons decrease with increasing temperature, as shown in Fig. 8. One possible explanation for this behavior is an increase of carrier concentration with temperature, thus providing a more effective screening of the phonons. We cannot derive, however, from our experimental results a unique temperature dependence of the free-carrier plasma frequency and therefore the carrier concentration in the framework of a Drude model (see next section). Available data from Hall measurements²⁶ are also controversial.

We showed in Fig. 3 the occurrence of the broad infrared reflectance band between 3000 and 6000 cm^{-1} , which has been reported by several groups.^{5,27} This band can be represented quite well by a Lorentzian with $\nu_e = 3100 \text{ cm}^{-1}$, $S_e = 50$, and $\Gamma_e = 4000 \text{ cm}^{-1}$.

V. ELECTRONIC RESPONSE

After analyzing the phonon structure of the FIR spectra of $\text{YBa}_2\text{Cu}_3\text{O}_{7-\delta}$ we shall try to get information about the underlying electronic part of the dielectric response by fitting it with a model dielectric function for $\hat{\epsilon}$. Because our measurements have been performed on nonoriented ceramic material, this function represents a spatial average value.

The phonon part $\hat{\epsilon}_{\text{PH}}$ was taken as a sum of Lorentzian oscillators with the parameters determined by the Kramers-Kronig analysis. For the electronic part we assumed above T_c a Drude-type response $\hat{\epsilon}_n$ and an additional oscillator $\hat{\epsilon}_e$, which represents the above-mentioned broad midinfrared band. Below T_c we used the Mattis-Bardeen approach for $\hat{\epsilon}_s$,²⁸ although it is at present unclear whether such an approximation is completely appropriate for the anisotropic high- T_c cuprates, because those materials have a coherence length ξ and a mean free path l with about the same order of magnitude, while the derivation of the Mattis-Bardeen theory is restricted to the extreme clean ($l \gg \xi$) and the extreme dirty ($l \ll \xi$) limit. Nevertheless, we hope to gain some understanding of the influence of various parameters on the final shape of reflectance spectra of $\text{YBa}_2\text{Cu}_3\text{O}_{7-\delta}$. We had, however, introduced a nonsuperconducting Drude part f_n of 10–20 % even at the lowest temperatures to fit

the reflectance data in the region around the 155- cm^{-1} phonon mode, although our x-ray analysis of the samples did not show such amount of another phase. It should be noted that the mm-wave absorption mentioned earlier (see Sec. III) is not in agreement with such a Drude part at low temperatures, because even an amount of 20% nonsuperconducting phase would result in a negligible absorption in the microwave region. We have to assume, therefore, that this last effect is intrinsic, e.g., in the sense of a nearly gapless region at the Fermi surface. On the other hand, the parameter f_n can be omitted, if one assumes that the frequency dependence of σ_1 is steeper above the onset of a gap than in the Mattis-Bardeen function. In order to account for an anisotropic character of the medium, without including too many parameters, we use in the fit two discrete gaps ν_{g1} and ν_{g2} . The slow increase of σ_1 (10 K) in Fig. 4 above 160 cm^{-1} suggests a superconductivity energy-gap distribution starting from that frequency up to a few hundred wave numbers, whereas for temperatures higher than T_c (120 K) the behavior is of Drude type. A possibility of gap anisotropy

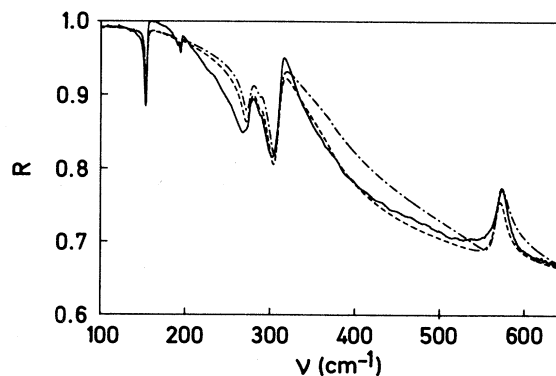


FIG. 9. Comparison between model dielectric function [Eq. (3)] and experiment at 10 K (solid line: experiment; dashed line: model dielectric function with parameters shown in Table V; dot-dashed line: the same function without the midinfrared contribution $\hat{\epsilon}_e$ and $\epsilon_\infty = 30$).

was inferred from NMR,²⁹ tunneling data,³⁰ and optical measurements.³¹ Below T_c the complex dielectric function can therefore be written as

$$\hat{\epsilon} = \epsilon_\infty + \hat{\epsilon}_e + \hat{\epsilon}_{\text{PH}}(T) + (1 - f_n)\hat{\epsilon}_S(T) + f_n\hat{\epsilon}_n(T). \quad (3)$$

The fit parameters for 10 K are given in Table V, and a comparison between the model and experimental results is shown in Fig. 9. To describe the temperature dependence in the low-frequency part of the spectra, we had to vary the Drude parameters ν_p and/or ν_τ , although the way they enter the dielectric function does not allow us to determine their detailed temperature dependence. Moreover, there are indications for a frequency-dependent scattering rate.² A value of a few thousand wave numbers is, however, a strong upper limit for the scattering frequency ν_τ , because it reduces the mean free path of the carriers to the interatomic distances. A crude estimation for ν_τ (around 600 cm^{-1}) can be deduced from the 120 K curve in Fig. 4, because σ_1 drops in the Drude picture at this frequency to half of its dc value. Attempts to fit the FIR spectra without assuming an additional oscillator $\hat{\epsilon}_e$ forced us to assume unphysically large values of ϵ_∞ . An example is also shown in Fig. 9. It turns out that the low-frequency tail of the midinfrared band significantly affects the shape of the phonon modes at 311 and 569 cm^{-1} , while the influence on the 154.8-cm^{-1} mode is negligible. The question of whether the midinfrared absorption peak is in any way related to the previously discussed anomalously high oscillator strength of the 154.8-cm^{-1} phonon^{32,33} remains open. However, at least in $\text{YBa}_2\text{Cu}_3\text{O}_{7-\delta}$, these features are both intimately related with the superconducting phase and may be connected with charge-transfer processes or their onset in the Cu(1)-O(IV) chains. The fitting procedure is definitely not unambiguous, but it should be stressed that

any fit in the framework of this model dielectric function without gaps (or a gap distribution) in the FIR region failed completely. Also, the extension of Eq. (3) to an anisotropic model with different gap values and Drude parameters for the a , b , and c directions requires a large oscillator strength ($S > 40$) for the 154.8-cm^{-1} mode, even when the conductivity in the c direction is reduced by a factor 100 as compared to the a - b -plane value.

We tried as well to apply effective medium theories³⁴⁻³⁶ to account for the anisotropy of the polycrystalline material. Due to the condition that the grain size L should be much smaller than the wavelength λ , this approximation is justified only in a frequency range up to roughly 200 cm^{-1} . Assuming such a theory³⁷ with a distribution of grain shapes leads also to this high oscillator strength value but, in contrast to the experiment, one obtains a broad and very asymmetric form for the 154.8-cm^{-1} phonon.

We conclude, therefore, that composite medium approaches are not appropriate to describe the reflectance behavior of these ceramics in the FIR region. Only the addition of the reflectivities³⁸ of a highly conducting a - b plane and a low (or not) conducting c direction including the Lorentzians for the phonons allows one to describe the observed spectra with much smaller oscillator strengths ($S \leq 1$ for all modes), but this requires $L \gg \lambda$, and this condition is not fulfilled in the present case.

ACKNOWLEDGMENTS

This work was supported by the Bundesministerium für Forschung und Technologie (Bonn, Germany). A.W. also acknowledges financial support from the Max-Planck Gesellschaft and the Polish Academy of Sciences (Research Project No. RPB-01-9).

*On leave of absence from Institute of Physics, Polish Academy of Sciences, aleja Lotnikow 32/46, PL-02-668 Warsaw, Poland.

¹Z. Schlesinger, R. T. Collins, D. L. Kaiser, F. Holtzberg, G. V. Chandrashekar, M. W. Shafer, and T. M. Plaskett, *Physica C* **153-155**, 1734 (1988).

²J. Orenstein, G. A. Thomas, D. H. Rapkine, A. J. Millis, L. F. Schneemeyer, and J. V. Waszczak, *Physica C* **153-155**, 1740 (1988).

³T. Timusk, D. A. Bonn, J. E. Greedan, C. V. Stager, J. D. Garrett, A. H. O'Reilly, and M. Reedyk, *Physica C* **153-155**, 1744 (1988).

⁴A. Wittlin, L. Genzel, M. Cardona, M. Bauer, H.-J. Mattausch, A. Simon, F. Garcia-Alvarado, E. Garcia, M. Barahona, and M. V. Cabanas, *Physica C* **153-155**, 663 (1988).

⁵K. Kamaras, C. D. Porter, M. G. Doss, S. L. Herr, D. B. Tanner, D. A. Bonn, J. E. Greedan, A. H. O'Reilly, C. V. Stager, and T. Timusk, *Phys. Rev. Lett.* **59**, 919 (1987).

⁶J. Orenstein and D. H. Rapkine, *Phys. Rev. Lett.* **60**, 968 (1988).

⁷G. A. Thomas, J. Orenstein, D. H. Rapkine, M. Capizzi, A. J.

Millis, R. N. Bhatt, L. F. Schneemeyer, and J. V. Waszczak, *Phys. Rev. Lett.* **61**, 1313 (1988).

⁸D. A. Bonn, A. H. O'Reilly, J. E. Greedan, C. V. Stager, T. Timusk, K. Kamaras, and D. B. Tanner, *Phys. Rev. B* **37**, 1574 (1988).

⁹W. Kress, U. Schroeder, J. Prade, A. D. Kulkarni, and F. W de Wette, *Phys. Rev. B* **38**, 2906 (1988).

¹⁰V. A. Maroni and R. Ferraro, in *Fourier Transform Infrared Spectroscopy in Industrial and Laboratory Analysis*, edited by J. R. Ferraro and K. Krishnan (Academic, New York, 1989).

¹¹M. Cardona, R. Liu, C. Thomsen, M. Bauer, L. Genzel, W. König, and A. Wittlin, *Solid State Commun.* **65**, 71 (1988).

¹²M. K. Crawford, W. E. Farneth, R. K. Bordia, and E. M. McCarron III, *Phys. Rev. B* **37**, 3371 (1988).

¹³C. Thomsen, H.-J. Mattausch, M. Bauer, W. Bauhofer, R. Liu, L. Genzel, and M. Cardona, *Solid State Commun.* **67**, 1069 (1988).

¹⁴J. P. Carini, A. M. Awasthi, W. Beyermann, G. Grüner, T. Hylton, K. Char, M. R. Beasley, and A. Kapitulnik, *Phys. Rev. B* **37**, 9726 (1988).

¹⁵R. S. Bauer, W. E. Spicer, and J. J. White III, *J. Opt. Soc.*

- Am. **64**, 830 (1974).
- ¹⁶U. Fano, Phys. Rev. **124**, 1866 (1961).
- ¹⁷M. Cardona, L. Genzel, R. Liu, A. Wittlin, H. J. Mattausch, F. Garcia-Alvarado, and E. Garcia-Gonzales, Solid State Commun. **64**, 727 (1987).
- ¹⁸J. W. Powell, G. S. Edwards, L. Genzel, F. Kremer, A. Wittlin, W. Kubasek, and W. Peticolas, Phys. Rev. A **35**, 3929 (1987).
- ¹⁹L. J. Sham and J. W. Wilkins, Phys. Rev. B **30**, 3062 (1984).
- ²⁰F. E. Pinkerton, B. C. Webb, A. J. Sievers, J. W. Wilkins, and L. J. Sham, Phys. Rev. B **30**, 3068 (1984).
- ²¹B. K. Chakraverty, D. Feinberg, Z. Hang, and M. Avignon, Solid State Commun. **64**, 1147 (1987).
- ²²B. K. Chakraverty, D. D. Sarma, and C. N. R. Rao, Physica C **156**, 413 (1988).
- ²³C. Thomsen, M. Cardona, W. Kress, R. Liu, L. Genzel, M. Bauer, and E. Schönherr, Solid State Commun. **65**, 1139 (1988).
- ²⁴A. Wittlin, R. Liu, M. Cardona, L. Genzel, W. König, W. Bauhofer, H. J. Mattausch, A. Simon, and F. Garcia-Alvarado, Solid State Commun. **64**, 477 (1987).
- ²⁵R. Zeyher and G. Zwirgmaier, Solid State Commun. **66**, 617 (1988).
- ²⁶S. W. Tozer, A. W. Kleinsasser, T. Penney, D. Kaiser, and F. Holtzberg, Phys. Rev. Lett. **59**, 1768 (1987).
- ²⁷T. Timusk and D. B. Tanner, in *Physical Properties of High Temperature Superconductors*, edited by D. M. Ginsberg (World-Scientific, Singapore, 1989), p. 339.
- ²⁸D. C. Mattis and J. Bardeen, Phys. Rev. **111**, 412 (1958).
- ²⁹W. W. Warren, Jr., R. E. Walstedt, G. F. Brennert, G. P. Espinosa, and J. P. Re, Phys. Rev. Lett. **59**, 1860 (1987).
- ³⁰J. S. Tsai, I. Takeuchi, J. Fujita, T. Yoshitake, S. Miura, S. Tanaka, T. Terashima, Y. Bando, K. Iigima, and K. Yamamoto, Physica C **153-155**, 1385 (1988).
- ³¹R. Hackl, W. Gläser, P. Müller, D. Einzel, and K. Andres, Phys. Rev. B **38**, 7133 (1988).
- ³²M. J. Rice and J. R. Wang, Phys. Rev. B **36**, 8794 (1987).
- ³³C. M. Varma, S. Schmitt-Rink, and E. Abrahams, Solid State Commun. **62**, 681 (1987).
- ³⁴D. A. G. Bruggeman, Ann. Phys. (Leipzig) **24**, 636 (1935).
- ³⁵L. Genzel and T. P. Martin, Surf. Sci. **34**, 33 (1973).
- ³⁶S. Hayashi, N. Nakamori, and H. Kanamori, J. Phys. Soc. Jpn. **46(1)**, 176 (1979).
- ³⁷T. E. Sulewski, T. W. Noh, J. T. McWhirter, and A. Sievers, Phys. Rev. B **36**, 5735 (1987).
- ³⁸Z. Schlesinger, R. T. Collins, M. W. Shafer, and E. M. Engler, Phys. Rev. B **36**, 5275 (1987).

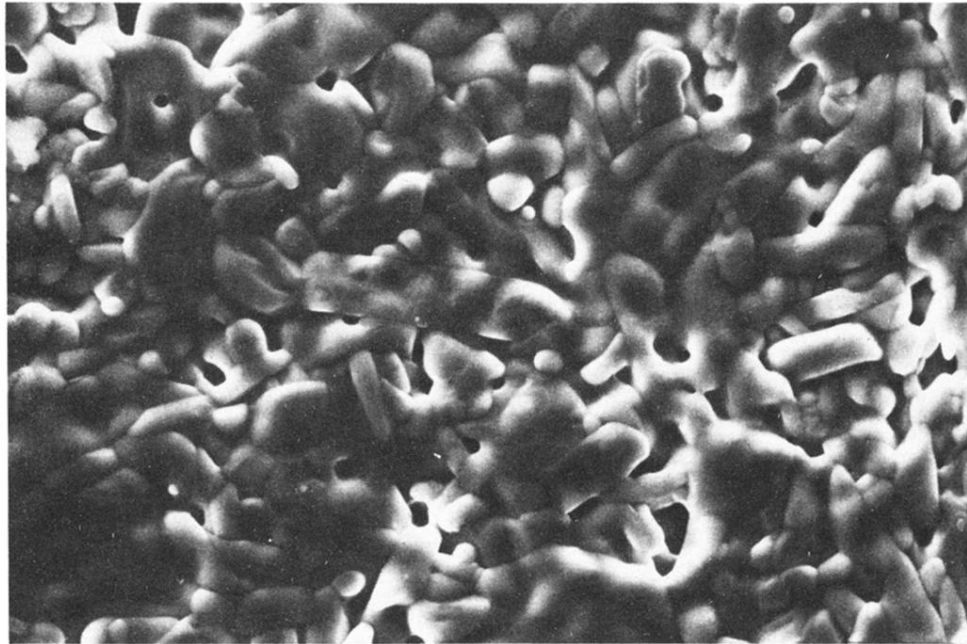


FIG. 2. Typical crystallite structure ($6\text{--}20\ \mu$ size) at the sample surface; the horizontal width of the figure corresponds to $80\ \mu$.